Physics Letters B 815 (2021) 136113

Contents lists available at ScienceDirect

Physics Letters B

www.elsevier.com/locate/physletb

Spectral distribution and Coulomb correction for nuclear bremsstrahlung induced by heavy targets

A. Mangiarotti [a,*], W. Lauth [b], D.H. Jakubassa-Amundsen [c], P. Klag [b], A.A. Malafronte [a], M.N. Martins [a], C.F. Nielsen [d], U.I. Uggerhøj [d]

[a] Instituto de Física da Universidade de São Paulo, Rua do Matão 1371, 05508-090 São Paulo, Brazil
[b] Institut für Kernphysik, Johannes Gutenberg Universität Mainz, 55099 Mainz, Germany
[c] Mathematics Institute, University of Munich, Theresienstrasse 39, 80333 Munich, Germany
[d] Department of Physics and Astronomy, Aarhus University, 8000 Aarhus, Denmark

ARTICLE INFO

Article history:
Received 14 September 2020
Received in revised form 25 January 2021
Accepted 28 January 2021
Available online 2 February 2021
Editor: M. Doser

Keywords:
Quantum electrodynamics
Bremsstrahlung
Photon spectra
Higher-order theory
Coulomb correction

ABSTRACT

Bremsstrahlung spectra below 250 MeV have been measured colliding 500 MeV–electrons with Cu, Ag, and Au targets. The experimental intensity ratios relative to Cu are well described by an accurate analytical high-energy theory, which accounts both for Coulomb distortion and screening. This represents the first experimental verification of the discovery by Bethe-Maximon that leading-order quantum mechanical calculations, equivalent to quasiclassical approximations, become exact at high energies and small angles. It also shows that radiative QED effects play a minor role in the covered part of the spectral distribution within the accuracy (1.6%) of the present measurements.

© 2021 The Author(s). Published by Elsevier B.V. This is an open access article under the CC BY license (http://creativecommons.org/licenses/by/4.0/). Funded by SCOAP[3].

1. Introduction

Nuclear bremsstrahlung is the simplest interaction mechanism between an electron and an atom involving the coupling to the radiation field. It is essentially the radiative correspondence to elastic scattering, to which it is related by the low-energy theorem [1,2]. This gave it a unique relevance at the dawn of Quantum Electrodynamics (QED). The first calculations were performed more than 80 years ago by Sommerfeld [3] for non-relativistic electrons, and by Sauter [4], Bethe and Heitler [5,6], and Racah [7] for relativistic electrons. Indeed, the prominent role continues to the present days. The most direct experimental evidences of phenomena beyond the standard formulation of QED, namely quantum coherence [8,9] (i.e. the Landau–Pomeranchuk–Migdal (LPM) suppression [10–13]), structured target resonance [14], and radiation back-reaction [15], were obtained within the context of nuclear bremsstrahlung. These phenomena are completely general and apply to every quantum theory of any interaction. However, a direct experimental proof was possible only in the case of QED, where the reference "standard" treatment is very well established [16–18] and allows to search for more subtle effects.

Bremsstrahlung investigations are transparent owing to three main reasons. *i*) The process can be treated as one body in an external field. *ii*) The momentum transfer is generally small and, therefore, the external field is well approximated as static and purely electric, even at high energies, since the cross section is dominated by the part of the phase space where the emitted photon and the final electron are strongly focused at small angles. *iii*) Radiative corrections are mostly negligible: for 5 GeV electrons, they were experimentally shown to be well below 1% for the lower 80% of the photon energy spectrum, increasing up to 5% close to its short–wavelength–limit (SWL) [19]. However, there emerge two difficulties.

The first one is a consequence of the formation length needed by the photon to be fully emitted (as proven by the existence of the LPM suppression). During the corresponding formation time, the electron continues to feel the static screened nuclear field. Therefore, the process cannot be described like a sequence of well separated localized interactions with either the static or the radiation fields, as it is necessary in standard perturbative QED, which is a theory of point interactions between free particles. Truly enough, a version of QED where a background field is present was developed and is known as the Furry picture of QED [20]. However, only the leading order was studied for bremsstrahlung and shown to

* Corresponding author.
E-mail address: alessio@if.usp.br (A. Mangiarotti).

https://doi.org/10.1016/j.physletb.2021.136113
0370-2693/© 2021 The Author(s). Published by Elsevier B.V. This is an open access article under the CC BY license (http://creativecommons.org/licenses/by/4.0/). Funded by SCOAP[3].

agree with the usual Fermi's golden rule. Nothing is known about the full perturbative expansion in the Furry picture.

The second difficulty is that the eigenfunctions of the Dirac equation corresponding to the continuous part of the spectrum do not possess a closed form even for a pure point-like Coulomb field. It is possible to use partial-wave expansions [21,22], but they become impractical above a few MeV because more than one million contributions to the matrix elements are needed to achieve convergence [23].

Experimental studies of high-energy bremsstrahlung are scarce. The existing data [8,9,14] are focused on the investigation of the LPM effect. Concerning the influence of the distortion of the wave function close to the nucleus, the original theory by Migdal [12] did not include the Coulomb correction, while that by Baier and Katkov [24] included it within the eikonal technique, which is equivalent to the leading order in the high-energy Bethe-Maximon approximation [25]. We note that a theory of quantum coherence effects taking into account higher-order corrections does not exist.

Experiments at medium-to-high energies [26,27] investigated the nuclear charge dependence of bremsstrahlung by considering targets ranging from copper to uranium at a single photon energy. To our knowledge, there is no measurement of the spectral distribution of the bremsstrahlung photons at collision energies above 100 MeV and below a few GeV. The latter limitation is imposed by the LPM suppression, which starts to change the shape of the measured spectrum [8,9]. Such experiments are needed to confirm the extended numerical tables for bremsstrahlung cross sections prepared by Seltzer and Berger [28,29] and currently adopted in all applications including simulation tools like Geant4 [30] and PENELOPE [31,32]. While for the low-energy regime (below 2 MeV) these tables are based on elaborate partial-wave calculations [21], for high energies (above 50 MeV) an interpolation technique is used to combine the analytical Bethe-Maximon theory [33] with the exact high-energy result at the SWL of the photon spectrum [34,35]. Special care is also necessary to join the regimes below 2 and above 50 MeV. Seltzer and Berger estimate the accuracy of Refs. [28,29] to be between 3 to 5% above 50 MeV. As a matter of fact, a comparison with advanced numerical quantum mechanical calculations [36] has revealed not negligible inaccuracies in these tables close to the SWL for electron energies beyond 50 MeV.

The present experiment at 500 MeV has been designed to extend the measurements by Brown [27], using the facilities of the MAMI accelerator at Mainz. The photon spectra up to 250 MeV are recorded, using thin foils of Cu, Ag, and Au in order to provide single-collision conditions. Concerning the LPM suppression, it affects only photons with an energy $\hbar\omega$ below [13]

$$\hbar\omega < \hbar\omega_{\mathrm{LPM}} = \frac{E_{\mathrm{beam}}(E_{\mathrm{beam}} - \hbar\omega)}{E_{\mathrm{LPM}}} \approx \frac{E_{\mathrm{beam}}^2}{E_{\mathrm{LPM}}} \qquad (1)$$

where E_{LPM} is a characteristic scale that depends on the material. For Gold, the worst case considered here, $E_{\mathrm{LPM}} = 2575$ GeV and $\hbar\omega_{\mathrm{LPM}} \approx 0.1$ MeV, well below the threshold accessible with the present setup.

These experimental data are compared to two conceptually different high-energy theories, available in analytical form. The first one is a quantum-mechanical theory, based on an extension of the Bethe-Maximon approach [33,37], while the second one is a quasiclassical approximation [38]. The equivalence of both theories relies on the fact that the lowest-order term of the respective wave functions coincide [39]. Besides the comparison with the measured spectral distributions, the effect of the Coulomb correction (which at 500 MeV has attained its high-energy limit and is accounted for in both theories) is also investigated by considering the ratio of the bremsstrahlung intensity for the various target species with respect to the one for copper.

2. Experiment at MAMI

The setup employed at MAMI was described elsewhere [40]. Here the main features are recalled. The continuous wave beam from MAMI-B (≈ 0.1-mm diameter and divergence much less than $1/\gamma$, where γ is the Lorentz factor of the electrons [40]) impinges on a thin foil mounted on a translation stage inside a vacuum chamber. Behind the target, the electrons are deflected by a first magnet and then bent by a series of other ones to end in a beam dump located below the floor. The photons are detected by a cylindrical NaI calorimeter with a diameter and a length of 10 inch, installed in a separate room behind a thick wall and enclosed in a lead shield. The initial path of the photons is kept in vacuum down to the mentioned wall [40]. A lead collimator is installed immediately in front of the calorimeter with an acceptance much larger than $1/\gamma$. Thus, considering the strong forward kinematic focusing, the measured spectrum reflects rather well the single differential cross section in photon energy. This setup results in a particularly low background that has allowed for the use of very thin metallic foils as targets. Those employed by Brown [27] had a thickness of $3 \cdot 10^{-2}$ of a radiation length (X_0), while, in the present case, the thickness is reduced to $5 \cdot 10^{-5}\, X_0$ (using self-supported films adhering to rigid stainless steel frames), thereby rendering negligible the spectral distortion due to the emission of multiple photons by a single electron crossing the target. On the other hand, Brown employed pion photoproduction on liquid hydrogen to identify the photons, which is insensitive to pile-up.

At these energies, there is no way to determine the response of the calorimeter to the high accuracy needed for the present experiment. In order to cancel the calorimeter response completely, it is necessary for the shape of the radiated photon spectrum to be similar to that of Cu. For this reason, Cu, Ag, and Au targets have been manufactured in large batches. Their thicknesses have been preliminary determined by Rutherford Back Scattering (RBS) at the LAMFI facility of the Institute of Physics of the University of São Paulo and then matched in sets with three targets having approximately the same thickness in units of X_0 (within $\approx \pm 20\%$). To take full advantage of the relative determination, during the runs the Ag or Au target has been exchanged four times with the reference one (Cu) to cancel possible drifts of the electronics or of the beam current (≈ 1 pA), which cannot be measured to the accuracy needed for the present experiment. Typical count rates have been kept around 5 kHz, resulting in dead time corrections of $\approx 2\%$. All spectra have been collected presetting the live time to 15 minutes. The data have been analysed in the following steps. *i*) The energy, k, deposited in the calorimeter, has been calibrated employing natural γ-lines and a ^{241}Am-^{9}Be source. *ii*) The background has been subtracted using a run taken with beam but without target. *iii*) The ratio of the Ag or Au to the Cu spectra, dN/dk, per interval of energy, dk, deposited in the calorimeter has been evaluated between each consecutive pair of measurements. *iv*) The ratios have been averaged. *v*) The average ratio has been corrected for the inverse ratio of the thickness, t (expressed in number of atoms per unit area), of the Ag or Au target to the reference one (Cu). *vi*) The average ratio has been corrected for the inverse ratio of the atomic numbers squared. Expressing all the previous steps in one formula gives

$$R_{i,\mathrm{Cu}}(k) = \left\langle \frac{\left(\frac{dN}{dk}\right)_i}{\left(\frac{dN}{dk}\right)_{\mathrm{Cu}}} \right\rangle \frac{t_{\mathrm{Cu}}\, Z_{\mathrm{Cu}}^2}{t_i\, Z_i^2} \ , \qquad (2)$$

where $i =$ Ag or Au. The results are shown in Fig. 1 for the target pairs of thickness $8 \cdot 10^{-5}\ X_0$ (filled squares ■): the flatness of

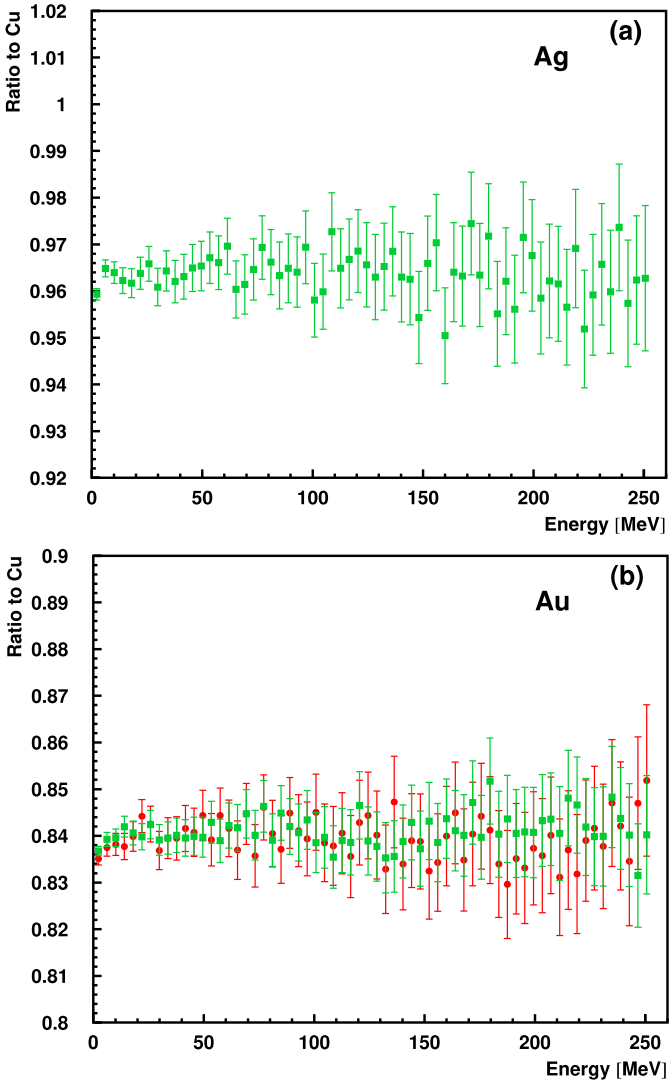

Fig. 1. Ratio defined in Eq. (2) for bremsstrahlung emission by impact of $E_{\text{beam}} = 500$ MeV electrons on (a) Ag ($Z = 47$) and (b) Au ($Z = 79$) as a function of the energy, k, deposited in the calorimeter. Target pairs of thickness $8 \cdot 10^{-5}$ X_0 have been measured for both Ag and Au (green filled squares ■). For Au, one additional pair of thickness $5 \cdot 10^{-5}$ X_0 has also been employed as a cross-check (red filled circles •). The error bars are statistical only (see the text for details).

$R_{i,\text{Cu}}$ as a function of k indicates that the pile-up and the response function of the calorimeter are indeed cancelled out. The decrease in the size of the error bars at low energies is due to the larger number of collected events following the well known approximate $1/k$ behaviour of the bremsstrahlung cross section.

The preparation of the targets, their storing in inert atmosphere to avoid excessive oxidation, and the determination of their thicknesses t has required the largest effort in setting up the experiment. After some investigations, it has been decided to finally extract t from the energy lost by α particles, emitted in the decay of ^{241}Am, while traversing the targets. To this end, a setup has been constructed, including a source holder, a collimator, a target insertion device, and a Passivated Implanted Planar Silicon (PIPS®) detector (manufactured by Canberra). A model for the response function of the PIPS detector has been developed to fit the recorded energy spectra of the α particles transmitted through the system. The ^{241}Am source has the extra complication of providing three main lines with slightly different energies (5.388, 5.443, and 5.486 MeV [41]) and very different intensities (corresponding, on average, to 1.66, 13.2, and 84.5 per hundred decays [41]), that have to be simultaneously taken into account in the fitting procedure. However, only the most intense line at 5.486 MeV has been used to evaluate the energy lost by the α particles, since its position can be obtained with the best accuracy, resulting in a more precise determination of the thickness of the target. To validate the method, calibration targets consisting of Al, Cu, Sn, and Au foils, manufactured by GoodFellow [42], have been employed. Their thicknesses have been determined by weighing with two micro-analytical balances and by measuring the area from images taken with a scanner to avoid distortions due to parallax. The uncertainty on the thicknesses of the calibration targets, estimated by propagating the uncertainties on the area and the weight (the former being dominant), is 0.5%. The directly measured results match, in the worst case, within 0.3% those obtained from the energy lost by α particles, when the ASTAR/NIST database, also available as the ICRU Report Number 49 [43], is adopted. This confirms the quality of the method, which has then been applied to the targets used at MAMI for the bremsstrahlung measurements, that are too fragile to be scanned and weighed. Key to achieving this precision has been the use of a low-activity open ^{241}Am source deposited as a very thin film on a substrate to reduce as much as possible energy loss and straggling in the source itself. A ^{232}Th source has also been employed to get calibration lines (including those from the ^{212}Po, ^{216}Po, ^{222}Rn, ^{212}Bi, ^{224}Ra, and ^{228}Th daughters) over a wide energy range from 3.9 to 8.8 MeV, covering the region where the peaks from the ^{241}Am one are displaced to because of the energy lost in the target foils. Last but not least, not all energy loss tabulations are adequate to reach the precision mentioned above: for example, the widely used SRIM code version 2013 [44] (the most recent available at the time of submission of this work) gives, for the calibration targets, a disagreement in the thickness that reaches up to 2% in the worst case (namely that of the Cu target). Thus, the ASTAR/NIST database has been preferred. A final verification that t has indeed been correctly determined is given in the lower panel of Fig. 1: another pair (red filled circles •) of Au and Cu targets has been employed at MAMI with t roughly half that of the first one (green filled squares ■) and a good agreement is observed in terms of $R_{\text{Au,Cu}}$. This is a crucial step to ensure that most of the relevant sources of systematic errors are indeed under control.

Once the ratio has been accurately determined, the differential cross sections for the two elements, Ag and Au, can be reconstructed by assuming the best calculations available for Cu (NLO with electron-electron bremsstrahlung correction, see Section 4) as displayed in Fig. 2. Once more, it has to be stressed that, at these energies, there is no way to determine the response of the calorimeter with high accuracy [8]. Thus, it is a common practice to use the lowest-Z data and theory, under the premise that the effects to be studied decrease with Z, to determine the absolute normalisation [9,14,15]. The systematic uncertainties affecting the data, much larger than the statistical ones displayed with error bars in Fig. 2, should also be added (see Fig. 3). Hence much effort has been devoted into an accurate determination of the Ag and Au spectra relative to Cu, in the spirit of extending the early measurements performed by Brown at a single photon energy. The actual values, together with their statistical uncertainties, are made available in tabular form in the supplementary material.

3. High-energy theory

Early bremsstrahlung calculations [4–7] were performed in the Plane Wave Born Approximation (PWBA), equivalent to standard perturbative QED. Much progress was since made by Sommerfeld and Maue [45] and Furry [46], who constructed closed form approximate solutions to the Dirac equation for a pure point-like Coulomb field. These Furry-Sommerfeld-Maue (FSM) wave functions, which become exact in the limit of high energies and large

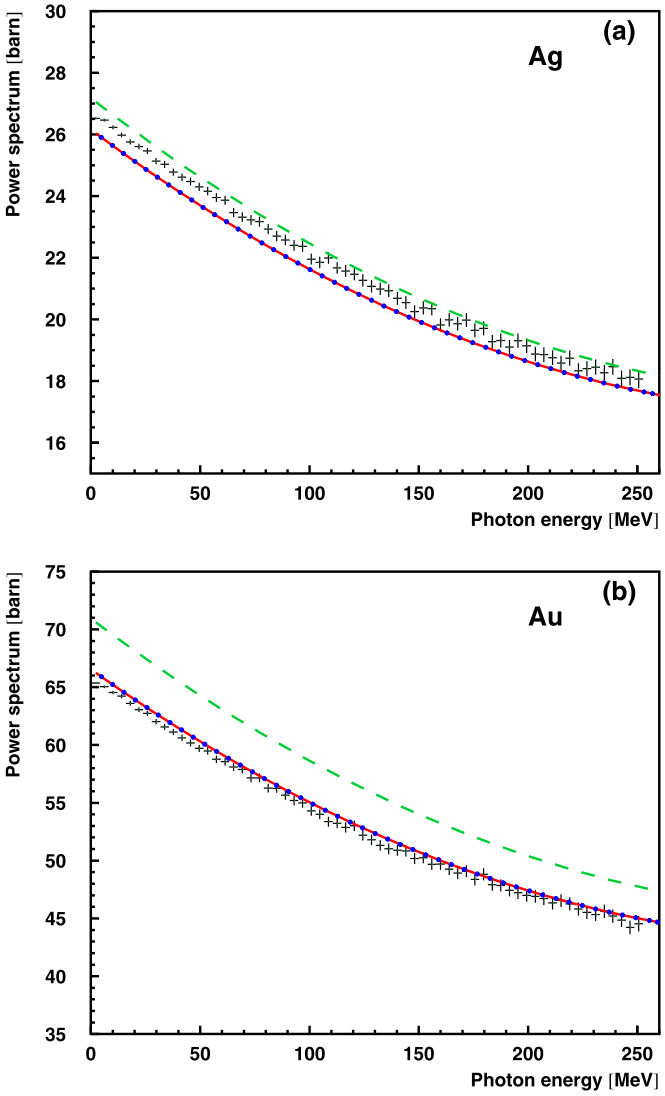

Fig. 2. Power spectrum ($\omega d\sigma/d\omega$) reconstructed from the data of Fig. 1 for the pairs of targets with thickness $8 \cdot 10^{-5}$ X_0 (histogram). The vertical bars represent the statistical uncertainties. Legend: LO (red, continuous curve), NLO (blue, dotted curve), and RDP (green, dashed curve) calculations.

angular momenta, represent for arbitrary conditions the leading order (LO) in αZ (with α the fine structure constant and Z the nuclear charge number) [17]. The distortion by the Coulomb field is partly accounted for at the LO, explaining the superiority of such an approach to the PWBA [17]. The FSM wave functions were first used by Bethe and Maximon in bremsstrahlung calculations [33]. Their results are valid under the approximations of high energies for the initial and final electrons and small angles. Later on, Elwert and Haug [47] removed those limitations obtaining an expression which is exact within the LO. It is adopted in the present work as well.

Upon adding a correction term ψ_c of order $(\alpha Z)^2$ to the FSM wave function $\psi_{\rm FSM}$ and inserting $\psi_{\rm FSM} + \psi_c$ into the Dirac equation, the bremsstrahlung matrix element M_c involving ψ_c was found analytically in the limit of high initial and final electron energies by Roche, Ducos, and Proriol [37]. In the next-to-leading order (NLO) approach, the absolute square of the radiation matrix element, determining the differential bremsstrahlung cross section, has to be calculated from

$$|M|^2_{\rm NLO} = |M_{\rm FSM}|^2 + 2\,{\rm Re}(M^\star_{\rm FSM}\, M_c) \ , \qquad (3)$$

where $M_{\rm FSM}$ is the matrix element in LO, evaluated with the FSM wave function. It is worth mentioning that Roche, Ducos, and Proriol (RDP) retained the term quadratic in M_c in the cross section [37], which belongs to the next-to-next-to leading order contributions. This RDP prescription leads to severe discrepancies with partial-wave bremsstrahlung calculations at backward angles for low collision energies where exact calculations are feasible [23]. Results from this RDP theory are included in Fig. 2, demonstrating its failure.

Alternative approaches to higher-order corrections are based on the quasiclassical theory. A WKB-type approximation, applied to each radial wave in the partial-wave expansion of the electronic scattering state leads (for a point-like Coulomb field) to the small-angle approximation of $\psi_{\rm FSM}$ [48]. On the other hand, an eikonal-type representation of the scattering state, obtained from an expansion in mc^2/E_i (where E_i is the total energy of the impinging electron) [38], reproduces to leading order the full Furry-Sommerfeld-Maue wave function [39]. For the angle-integrated photon spectrum, the use of the corresponding quasiclassical Green's function leads to a simple analytical expression, including the leading order and the next-to-leading order in mc^2/E_i [39]. This new approach results in more manageable expressions but employs the approximations of high energies for the initial and final electrons and small angles. Moreover, it continues to rely on Fermi's golden rule and thus does not improve the traditional one as far as a unified treatment of radiative and non-radiative corrections is concerned. We stress that the LO quantum calculations shown here do not involve any high-energy or small-angle approximations. The NLO ones are also not limited to small angles. The high-energy assumption is, however, implied by the form of ψ_c adopted in Ref. [37].

Screening by the target electrons can easily be accounted for in the quasiclassical theory, since the target potential enters explicitly into the formula for the bremsstrahlung cross section [38]. In the quantum mechanical NLO approach, screening is considered by means of the Olsen-Maximon-Wergeland (OMW) additivity rule [48,49], which profits from the fact that Coulomb distortion and screening effects are important in different spatial regions, allowing to calculate the screening correction in the PWBA.

Bethe and Maximon [33] found that, in the limit of ultrahigh energies and at small observation angles, the FSM wave function becomes exact, irrespective of αZ being small. Actually it can be shown that the convergence of the FSM wave function to the exact solution with increasing energy is not uniform, since the bound of the difference between the two functions at a point in space depends on the distance from the origin of the Coulomb field as well as on the angle between the electron momentum and the displacement vector from the origin. This renders exact analytical studies difficult. The Bethe–Maximon classification of the order in αZ and the energy dependence of the various contributions to the cross section, being the most complete to the present day, relies, however, on the high-energy and small-angle approximations.

Concerning the importance of higher-order corrections, it is well-known that the FSM theory fails at the high-energy end of the spectrum where the scattered electron is very slow. In contrast, the quantum mechanical higher-order approaches provide a correction at the SWL in accord with low-energy exact calculations [36,50]. On the other hand, the quasiclassical corrections diverge at the SWL [39]. This deficiency can, however, be remedied by applying the quasiclassical approximation only to the incoming electron, while treating the slow outgoing electron quantum mechanically [51]. In the following section, we provide a comparison of the quantum mechanical and the quasiclassical theory with the data for the lower half of the photon spectrum.

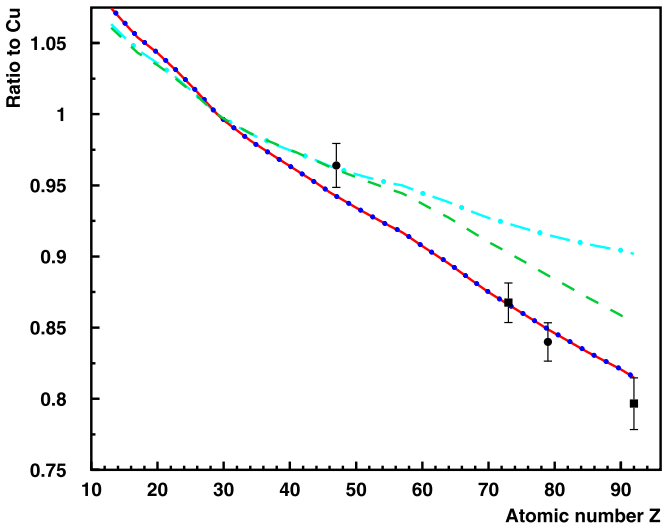

Fig. 3. Comparison of the theory ratio from Eq. (4) with $\hbar\omega = 234$ MeV to the experimental ratio from Eq. (2) as a function of the atomic number of the target. The experimental points are from Brown [27] (filled squares ■) and the present work (filled circles •). In the latter case, where it is possible to check that Eq. (2) does not depend on k, an average is taken to reduce the statistical uncertainty to a negligible level. Legend: PWBA (cyan, dot-dashed curve), LO (red, continuous curve), NLO (blue, dotted curve), and RDP (green, dashed curve) calculations.

4. Comparison of experiment with theory

In all the theoretical approaches considered (i.e. LO, NLO, and RDP), the ratio

$$R_{i,\mathrm{th}}(\omega) = \frac{\left(\frac{d\sigma}{d\omega}\right)_i Z_{\mathrm{Cu}}^2}{\left(\frac{d\sigma}{d\omega}\right)_{\mathrm{Cu}} Z_i^2} \ , \tag{4}$$

where $i =$ Ag or Au, and $d\sigma/d\omega$ is the single differential cross section for the emission of a photon with energy $\hbar\omega$, is expected to be flat away from the SWL. In such a case, it is possible to compare $R_{i,\mathrm{Cu}}$ with $R_{i,\mathrm{th}}$ without having to deconvolve the response of the detector. It is then legitimate to employ the weighted average of the measured $R_{i,\mathrm{Cu}}(k)$ (0.964 for Ag and 0.840 for Au), affected by a negligible statistical error, to compare with the constant value of R_{th}, as shown in Fig. 3. The agreement of the present data with those by Brown [27] is very good considering the error bars, which represent the systematic alone and the total uncertainty [27] for the former and latter cases, respectively. The present systematic error is estimated to be 1.6% due to the uncertainty in t (0.5% as estimated from the uncertainty in the thickness of the reference targets), the uniformity of the target (1% as checked at MAMI with a beam scan over the target surface), and the reproducibility (0.1% as evaluated from the standard deviation of the average appearing in Eq. (2), most likely due to an uncompensated time drift of the unmeasured beam current).

Clearly, the PWBA, equivalent to the standard perturbative QED, completely fails to reproduce the data and gives a too high cross section (by $\approx 10\%$) at large Z. By the way, the PWBA is not constant in Z (one might expect that $R_{i,\mathrm{th}}(\omega) = 1$ independent of Z) because of the presence of screening (which is taken into account using Dirac-Hartree-Fock-Slater form factors made available as part of the RTAB database by Kissel [52]). The small contribution of electron-electron bremsstrahlung has been included in Eq. (4) by a bilinear interpolation in log-log scale of the tables published by Seltzer and Berger [28,29].

The same PWBA is employed to add screening to the LO, NLO, and RDP results according to the OMW prescription as mentioned. Electron-electron bremsstrahlung is included as described. The RDP theory, applied so far in all the published literature on this matter [37,53,54] except Ref. [23], is also not consistent with the data and should be rejected in all further calculations both at low energies, as demonstrated in Ref. [23], and in the high-energy limit according to the present work. On the other hand, the NLO scheme proposed in Ref. [23] agrees with the LO in the high-energy limit and with the data. The calculations shown in Fig. 3, which required the evaluation of the single differential cross section as function of ω for a grid of atomic numbers containing one every three elements (29 in total including Cu, Ag, Ta, Au, and U) demanded about two years of CPU time on a modern multi core 64-bit unit running at 2.0 GHz (opteron 6128 HE manufactured by AMD®). All the numerical aspects of the program were thoroughly tested, as described in Ref. [55]. The agreement of the LO and NLO results, some tens of MeV away from the SWL, is found to be within the requested relative numerical accuracy of the calculations (10^{-4}). Discrepancies of the same order of magnitude are present in the lower half of the photon energy spectrum, when considering the leading order and the next-to-leading order of the quasiclassical approach [39]. These differences increase in the upper half towards the SWL, not covered by the present data, because of the additional high-energy and small-angle approximations, employed in Ref. [39], which are invalid for the final state. The comparison of the LO calculations with the tables by Seltzer and Berger [28,29] requires some cautions and was discussed in Ref. [18]. For the electron energies of interest here, the lower half of the spectrum, and the case of low Z, the agreement is limited by the published number of significant figures. The discrepancy increases, under the same conditions, towards higher Z to reach close to the level of the systematic uncertainty of the present data, around 1%. It is most probably due to the use of different atomic form factors.

5. Conclusion

The RDP prescription, where of all the terms contributing to the next-to-next-to leading order only $|M_{\mathrm{c}}|^2$ is retained and which was used in all previously published literature on the quantum theory, is shown to be in disagreement with the experimental data presented in Figs. 2 and 3, remaining well outside of their uncertainties. The contrary is true for the consistent NLO truncation scheme, proposed in Ref. [23]. The results displayed here also represent the first experimental and numerical verification (avoiding the small-angle approximation) of the Bethe-Maximon discovery that the bremsstrahlung theory, based on the FSM wave functions, becomes exact at high energies, implying that the higher-order (non-radiative) contributions to the Coulomb correction vanish. Thus, such a result fully justifies the eikonal technique, which is equivalent to the LO, used to study quantum coherence and radiation back reaction effects. Moreover, in the photon energy domain probed by the present data, it has been shown numerically that the LO theory, based on an expansion of the electronic wave function in terms of αZ at high energy, and the quasiclassical approach by Lee and coworkers [39], which results from a corresponding expansion in mc^2/E_i, within the leading order and the next-to-leading order approximation, are equivalent. Current cross section tables [28,29] agree with the data considering the systematic uncertainties quoted above.

The data presented in Fig. 3 leave only a rather small space at very high Z for the presence of other effects, like radiative or higher-order screening corrections, but new measurements with more targets and an improved control over systematic uncertainties are necessary to firmly establish such a conclusion. Future investigations covering the full spectrum up to the SWL are planned to study radiative corrections, the accuracy of available tables, and the validity of the quasiclassical approaches. However, this requires mastering the deconvolution of the response function of the

calorimeter at the level of few percent. Note that the use of simulation tools, like Geant4, to determine the response function of the calorimeter inevitably relies on a choice of a theoretical description of bremsstrahlung ending up in a somewhat circular procedure, which has been fully avoided in the present work by the measurements relative to Cu.

Declaration of competing interest

The authors declare that they have no known competing financial interests or personal relationships that could have appeared to influence the work reported in this paper.

Acknowledgements

The technical staffs of MAMI and LAMFI-IFUSP are acknowledged for the smooth operation of the respective accelerators. The authors are grateful to Drs. W. G. P. Engel and A. C. Tromba for preparing the targets by evaporation at Laboratório de Alvos Nucleares-IFUSP, to Prof. Dr. T. F. Silva for the analysis of their thicknesses by Rutherford back scattering with the data collected at LAMFI-IFUSP, to Dr. A. R. Petri for help with the analysis of the α-particle spectra, to Dr. J. Ahrens for fruitful discussions about the setup at MAMI, to Profs. Drs. A. A. F. S. Kerr and H. M. J. Barbosa for granting access to their respective installations with microanalytical balances, and to Mr. L. A. de Queiroz e Silva for assistance with the conversion of the tables by Seltzer and Berger to digital form. They are in debt with Profs. Drs. G. Burdman, E. M. Santos, P. Sona, and A. Olmi for reading earlier versions of the present manuscript and making valuable suggestions. AM remembers his father, who passed away shortly after the measurements. This work has been supported by Fundação de Amparo à Pesquisa do Estado de São Paulo (FAPESP) under Contracts No. 2013/15634-5 and No. 2016/13116-5, by Conselho Nacional de Desenvolvimento Científico e Tecnológico (CNPq) under Contract No. 306331/2016-0, and by the European Union's Horizon 2020 research and innovation programme under grant agreement STRONG 2020 - No. 824093. By making the experimental bremsstrahlung spectra available to other researchers in the same form presented in this paper, we are fulfilling the Data Management Plan in accordance to the guidelines defined by FAPESP.

Appendix A. Supplementary material

Supplementary material related to this article can be found online at https://doi.org/10.1016/j.physletb.2021.136113.

References

[1] F.E. Low, Bremsstrahlung of very low-energy quanta in elementary particle collisions, Phys. Rev. 110 (1958) 974.
[2] T.H. Burnett, N.M. Kroll, Extension of the low soft-photon theorem, Phys. Rev. Lett. 20 (1968) 86.
[3] A. Sommerfeld, Über die Beugung und Bremsung der Elektronen, Ann. Phys. 11 (1931) 257.
[4] F. Sauter, Über die Bremsstrahlung schneller Elektronen, Ann. Phys. 20 (1934) 404.
[5] H.A. Bethe, W. Heitler, On the stopping of fast particles and on the creation of positive electrons, Proc. R. Soc. Lond. Ser. A 146 (1934) 83.
[6] H.A. Bethe, The influence of screening on the creation and stopping of electrons, Proc. Camb. Philos. Soc. 30 (1934) 524.
[7] G. Racah, Sopra l'irradiazione nell'urto di particelle veloci, Nuovo Cimento 11 (1934) 461.
[8] P.L. Anthony, R. Becker-Szendy, P.E. Bosted, M. Cavalli-Sforza, L.P. Keller, L.A. Kelley, S.R. Klein, G. Niemi, M.L. Perl, L.S. Rochester, J.L. White, An accurate measurement of the Landau-Pomeranchuk-Migdal effect, Phys. Rev. Lett. 75 (1995) 1949.
[9] H.D. Hansen, U.I. Uggerhøj, C. Biino, S. Ballestrero, A. Mangiarotti, P. Sona, T.J. Ketel, Z.Z. Vilakazi, Is the electron radiation length constant at high energies?, Phys. Rev. Lett. 91 (2003) 014801.
[10] L.D. Landau, I.J. Pomeranchuk, The limits of applicability of the theory of bremsstrahlung by electrons and of the creation of pairs at high energy, Dokl. Akad. Nauk SSSR 92 (1953) 535, available in English in L. D. Landau, The collected papers of L. D. Landau, edited by D. Ter Haar, Pergamon, 1965, page 586.
[11] L.D. Landau, I.J. Pomeranchuk, Electron cascade processes at ultra-high energies, Dokl. Akad. Nauk SSSR 92 (1953) 735, available in English in L. D. Landau, The collected papers of L. D. Landau, edited by D. Ter Haar, Pergamon, 1965, page 589.
[12] A.B. Migdal, Bremsstrahlung and pair production in condensed media at high energies, Phys. Rev. 103 (1956) 1811.
[13] S. Klein, Suppression of bremsstrahlung and pair production due to environmental factors, Rev. Mod. Phys. 71 (1999) 1501.
[14] K.K. Andersen, S.L. Andersen, J. Esberg, H. Knudsen, R. Mikkelsen, U.I. Uggerhøj, P. Sona, A. Mangiarotti, T.J. Ketel, S. Ballestrero, Direct measurement of the formation length of photons, Phys. Rev. Lett. 108 (2012) 071802.
[15] T. Wistisen, A. Di Piazza, H.V. Knudsen, U.I. Uggerhøj, Experimental evidence of quantum radiation reaction in aligned crystals, Nat. Commun. 9 (2018) 795.
[16] H.W. Koch, J.W. Motz, Bremsstrahlung cross-section formulas and related data, Rev. Mod. Phys. 31 (1959) 920.
[17] E. Haug, W. Nakel, The Elementary Process of Bremsstrahlung, 1st edition, World Scientific, Singapore, 2004.
[18] A. Mangiarotti, M.N. Martins, A review of electron–nucleus bremsstrahlung cross sections between 1 and 10 MeV, Radiat. Phys. Chem. 141 (2017) 312.
[19] H.D. Schulz, G. Lutz, Experimental confirmation of radiative corrections to bremsstrahlung and pair production at high energy, Phys. Rev. 167 (1968) 1280.
[20] J.M. Jauch, F. Rohrlich, The Theory of Photons and Electrons, Addison-Wesley, Cambridge, Massachusetts, 1955.
[21] H.K. Tseng, R.H. Pratt, Exact screened calculations of atomic-field bremsstrahlung, Phys. Rev. A 3 (1971) 100.
[22] V.A. Yerokhin, A. Surzhykov, Electron-atom bremsstrahlung: double-differential cross section and polarization correlations, Phys. Rev. A 82 (2010) 062702.
[23] D.H. Jakubassa-Amundsen, A. Mangiarotti, Accuracy of analytical theories for relativistic bremsstrahlung, Phys. Rev. A 100 (2019) 032703.
[24] V.N. Baier, V.M. Katkov, Concept of formation length in radiation theory, Phys. Rep. 409 (2005) 261.
[25] R. Blankenbecler, S.D. Drell, The Bethe–Maximon result, Phys. Rev. D 36 (1987) 2846.
[26] W.C. Barber, A.I. Berman, K.L. Brown, W.D. George, Z-dependence of bremsstrahlung, Phys. Rev. 99 (1955) 59.
[27] K.L. Brown, Z dependence of bremsstrahlung for the case of complete screening, Phys. Rev. 103 (1956) 243.
[28] S.M. Seltzer, M.J. Berger, Bremsstrahlung spectra from electron interactions with screened atomic nuclei and orbital electrons, Nucl. Instrum. Methods Phys. Res. B 12 (1985) 95.
[29] S.M. Seltzer, M.J. Berger, Bremsstrahlung energy spectra from electrons with kinetic energy 1 keV–10 GeV incident on screened nuclei and orbital electrons of neutral atoms with $Z = 1$–100, At. Data Nucl. Data Tables 35 (1986) 345.
[30] S. Agostinelli, et al., Geant4–a simulation toolkit, Nucl. Instrum. Methods Phys. Res. A 506 (2003) 250.
[31] J. Baró, J. Sempau, J.M. Fernández-Varea, F. Salvat, PENELOPE: an algorithm for Monte Carlo simulation of the penetration and energy loss of electrons and positrons in matter, Nucl. Instrum. Methods Phys. Res. B 100 (1995) 31.
[32] J. Sempau, E. Acosta, J. Baró, J.M. Fernández-Varea, F. Salvat, An algorithm for Monte Carlo simulation of coupled electron-photon transport, Nucl. Instrum. Methods Phys. Res. B 132 (1997) 377.
[33] H.A. Bethe, L.C. Maximon, Theory of bremsstrahlung and pair production. I. Differential cross section, Phys. Rev. 93 (1954) 768.
[34] R.J. Jabbur, R.H. Pratt, High-frequency region of the spectrum of electron and positron bremsstrahlung, Phys. Rev. 129 (1963) 184.
[35] R.J. Jabbur, R.H. Pratt, High-frequency region of the spectrum of electron and positron bremsstrahlung II, Phys. Rev. 133 (1964) B1090.
[36] D.H. Jakubassa-Amundsen, An asymptotic DSM theory for high-energy near-tip bremsstrahlung, J. Phys. G 47 (2020) 075102.
[37] G. Roche, C. Ducos, J. Proriol, Bremsstrahlung cross-section formula including a high-order Coulomb correction, Phys. Rev. A 5 (1972) 2403.
[38] R.N. Lee, A.I. Milstein, V.M. Strakhovenko, Quasiclassical Green function in an external field and small-angle scattering processes, J. Exp. Theor. Phys. 90 (2000) 66.
[39] R.N. Lee, A.I. Milstein, V.M. Strakhovenko, O.Ya. Schwartz, Coulomb corrections to bremsstrahlung in the electric field of a heavy atom at high energies, J. Exp. Theor. Phys. 100 (2005) 1.
[40] H. Backe, D. Krambrich, W. Lauth, J.L. Hansen, U.I. Uggerhøj, X-ray emission from a crystal undulator–experimental results at channeling of electrons, Nuovo Cimento 34C (2011) 157.
[41] M.-M. Bé, V. Chisté, C. Dulieu, X. Mougeot, E. Browne, V. Chechev, N. Kuzmenko, F. Kondev, A. Luca, M. Galán, A.L. Nichols, A. Arinc, X. Huang, Table of Radionuclides, Monographie BIPM-5, vol. 5, Bureau International des Poids et Mesures, Pavillon de Breteuil, F-92310 Sèvres, France, 2010, http://www.bipm.org/utils/common/pdf/monographieRI/Monographie_BIPM-5_Tables_Vol5.pdf.

[42] Goodfellow Cambridge Limited, http://www.goodfellow.com/pdf/3057_1111010.pdf.
[43] M.J. Berger, M. Inokuti, H.H. Andersen, H. Bichsel, D. Powers, S.M. Seltzer, D. Thwaites, D.E. Watt, Report 49: stopping powers and ranges for protons and alpha particles, J. ICRU os25 (2) (1993), https://doi.org/10.1093/jicru/os25.2.Report49.
[44] J.F. Ziegler, M.D. Ziegler, J.P. Biersack, SRIM – the stopping and range of ions in matter (2010), Nucl. Instrum. Methods Phys. Res. B 268 (2010) 1818.
[45] A. Sommerfeld, A.W. Maue, Verfahren zur näherungsweisen Anpassung einer Lösung der Schrödinger- an die Diracgleichung, Ann. Phys. (Leipz.) 22 (1935) 629.
[46] W.H. Furry, Approximate wave functions for high energy electrons in Coulomb fields, Phys. Rev. 46 (1934) 391.
[47] G. Elwert, E. Haug, Calculation of bremsstrahlung cross sections with Sommerfeld-Maue eigenfunctions, Phys. Rev. 183 (1969) 90.
[48] H. Olsen, L.C. Maximon, H. Wergeland, Theory of high-energy bremsstrahlung and pair production in a screened field, Phys. Rev. 106 (1957) 27.
[49] H. Olsen, Outgoing and ingoing waves in final states and bremsstrahlung, Phys. Rev. 99 (1955) 1335.
[50] D.H. Jakubassa-Amundsen, The DSM theory for tip electron-atom bremsstrahlung at 5–500 MeV, Radiat. Phys. Chem. 162 (2019) 172.
[51] A. Di Piazza, A.I. Milstein, High-energy electron-positron photoproduction cross section close to the end of the spectrum, Phys. Rev. A 82 (2010) 042106.
[52] L. Kissel, RTAB: the Rayleigh scattering database, Radiat. Phys. Chem. 59 (2000) 185.
[53] E. Haug, Bremsstrahlung cross-section with screening and Coulomb corrections at high energies, Radiat. Phys. Chem. 77 (2008) 207.
[54] A. Mangiarotti, M.N. Martins, Higher–order corrections to electron–nucleus bremsstrahlung cross sections above a few MeV, Phys. Rev. A 94 (2016) 022708.
[55] A. Mangiarotti, M.N. Martins, V.R. Vanin, Analytic calculations of electron–nucleus bremsstrahlung cross sections above a few MeV including higher-order corrections and multiple scattering in the target, Nucl. Instrum. Methods Phys. Res. B 446 (2019) 58.